Scaled momentum distributions of charged particles in dijet photoproduction at HERA

John Morris

Queen Mary University of London - Dept of Physics, Mile End Road, London - UK

The scaled momentum distributions of charged particles in jets have been measured for dijet photoproduction with the ZEUS detector at HERA using an integrated luminosity of 359 pb^{-1}. The distributions are compared to predictions based on perturbative QCD carried out in the framework of the modified leading-logarithmic approximation (MLLA) and assuming local parton-hadron duality (LPHD). The universal MLLA scale, $\Lambda_{\rm eff}$, and the LPHD parameter, $\kappa^{\rm ch}$, are extracted.

1 The MLLA framework

The modified leading-logarithmic approximation (MLLA) [1] is an all orders resummation approach to perturbative QCD (pQCD). The MLLA includes all terms of order $\alpha_s^n \log^{2n}(E^{\rm pl}_{\rm init})$ and $\alpha_s^n \log^{2n-1}(E^{\rm pl}_{\rm init})$, where n is the set of positive integers and $E^{\rm pl}_{\rm init}$ is the energy of the initial outgoing parton in the centre-of-mass frame of the incoming struck parton and exchanged photon. The "pl" superscript denotes a parton-level quantity. The MLLA may only be used to describe partons at scales above some minimum cutoff, $\Lambda_{\rm eff} > \Lambda_{\rm QCD}$. The value of $\Lambda_{\rm eff}$ is predicted to be independent of the process considered. The local parton hadron duality (LPHD) [2] hypothesis predicts that charged-hadron distributions should be related to the predicted parton distributions by a constant normalisation scaling factor, $\kappa^{\rm ch}$.

The shape of the predicted spectrum depends on the quantity, $Y = \ln(E^{\rm pl}_{\rm init}\sin(\theta^{\rm pl}_c)/\Lambda_{\rm eff})$. The spectrum is roughly Gaussian, although, due to the regularisation scheme adopted, falls rapidly to zero as $\xi^{\rm pl} \to Y$. At leading order (LO), the peak position of the limiting momentum spectrum, $\xi^{\rm pl}_{\rm peak}$, is predicted to be at

$$\xi^{\rm pl}_{\rm peak} = \frac{1}{2}Y + \sqrt{cY} - c, \tag{1}$$

where $c = 0.29$. Photoproduction samples contain both gluon- and quark-initiated jets, in the fractions denoted by $\epsilon_{\rm g}$ and $\epsilon_{\rm q} = 1 - \epsilon_{\rm g}$, respectively. The limiting spectrum for partons in all jets can be parameterised as

$$\bar{D}^{\rm lim,pl} = \left(\epsilon_{\rm g} + \frac{1-\epsilon_{\rm g}}{r}\right)\bar{D}^{\rm lim,pl}_{\rm g-jet}. \tag{2}$$

where $r = N^{\rm pl}_{\rm g-jet}/N^{\rm pl}_{\rm q-jet}$ is the ratio of parton multiplicities in gluon- and quark-initiated jets. Solutions to the MLLA evolution equations have also been made at so-called next-to-MLLA [4] order where $F_{\rm nMLLA}$ and r differ from their MLLA values and both have a weak dependence on $E^{\rm pl}_{\rm init}$. Their values were taken from three different next-to-MLLA calculations, which differ in the way the additional orders are accounted for, leading to some spread in the predicted $F_{\rm nMLLA}$ and r values. Here, constant values of $F_{\rm nMLLA} = 1.3 \pm 0.2$ and $r = 1.6 \pm 0.2$ were used, with the theoretical uncertainties covering the spreads.

The LPHD approximation relates the limiting momentum spectrum of partons to that of charged hadrons within jets, $\bar{D}^{\rm lim,ch}$. Due to isospin invariance, it is expected that $\kappa^{ch} \approx 2/3$.

$$\bar{D}^{\mathrm{lim,ch}} = \kappa^{\mathrm{ch}} \bar{D}^{\mathrm{lim,pl}} = \kappa^{\mathrm{ch}} \left(\epsilon_{\mathrm{g}} + \frac{1-\epsilon_{\mathrm{g}}}{r} \right) \bar{D}^{\mathrm{lim,pl}}_{\mathrm{g-jet}} = K \bar{D}^{\mathrm{lim,pl}}_{\mathrm{g-jet}}, \quad (3)$$

2 Data analysis

To compare the parton-level MLLA predictions to measured hadron-level data, while assuming LPHD, each variable within the MLLA had to be estimated using a related hadron-level quantity. The hadron-level estimator for $E^{\mathrm{pl}}_{\mathrm{init}}$ was chosen to be $E_{\mathrm{jet}} = M_{2j}/2$, where E_{jet} is the energy of either hadron-level jet in the dijet centre-of-mass frame and M_{2j} is the invariant dijet mass. The quantity p^{pl}_{p} was estimated using the momenta of the charged hadrons, p_{trk}. The loss of the neutral hadrons is accounted for via the LPHD factor κ^{ch}. The MLLA variable θ^{pl}_{c} was estimated using the opening angle of a cone measured with respect to the reconstructed jet axis, θ_c. Accordingly, the quantity $\bar{D}^{\mathrm{lim,ch}}$, given in Eq. 3, was estimated using the hadron-level multiplicity distribution of charged hadrons per jet, $N^{\mathrm{ch}}_{\mathrm{jet}}$, measured in bins of E_{jet} and in cones of varying θ_c, differentially in $\xi = \ln\left(E_{\mathrm{jet}}/|p_{\mathrm{trk}}|\right)$. These $\mathrm{d}N^{\mathrm{ch}}_{\mathrm{jet}}/\mathrm{d}\xi$ distributions will be referred to as the ξ distributions.

The data analysed here were collected using the ZEUS detector during the 2005 to 2007 running periods, in which electrons[a] were collided with protons with energies of $E_e = 27.5\,\mathrm{GeV}$ and $E_p = 920\,\mathrm{GeV}$, respectively, corresponding to a centre-of-mass energy, $\sqrt{s} = 318\,\mathrm{GeV}$. The total sample corresponds to an integrated luminosity of 359 ± 9 pb^{-1}. A detailed description of the ZEUS detector can be found elsewhere [5].

The data were selected such that 2 and only 2 jets were found with an $|\eta| < 1.0$ The hardest jet was required to have $E_T^{\mathrm{Jet}\,1} \geq 17\,\mathrm{GeV}$ and a ratio of $E_T^{\mathrm{Jet}\,2}/E_T^{\mathrm{Jet}\,1} \geq 0.8$ and $0.9\pi \leq |\phi^{\mathrm{Jet}\,1} - \phi^{\mathrm{Jet}\,2}|$ was imposed. The phase space was restricted to $0.2 \leq y \leq 0.85$, $Q^2 \leq 1\,\mathrm{GeV}$ and $x_{\gamma}^{OBS} \geq 0.75$. All tracks considered were required to have $p_T \geq 150\,\mathrm{MeV}$ and $|\eta| \leq 1.7$. Monte Carlo truth charged particles were considered stable if they had a lifetime $\geq 0.01ns$. After all the above selection, the data sample contained 23,449 events.

3 Results and discussion

The ξ distributions were measured in five bins of $E_{\mathrm{jet}} = \{19, 23, 28, 32, 38\}$ GeV and in cones around the reconstructed jet axes with opening angles $\theta_c = \{0.23, 0.28, 0.34\}$. The $\theta_c = 0.23$ ξ distributions are shown in Fig. 1 (a). Each of the distributions are observed to be similar in shape and are roughly Gaussian with more pronounced upper tails. To assess the validity of the MLLA predictions using the measured ξ distributions, two approaches were adopted. The first was based solely on the position of the peak of the ξ distributions, ξ_{peak}. The second was based on the full shape of the ξ distributions.

The values of ξ_{peak} were extracted from the ξ distributions using a three-parameter Gaussian fit in the range $\mu_\xi \pm 1$, where μ_ξ is the arithmetic mean of the ξ distribution.The χ^2/dof values range between 0.48 and 1.33 and hence indicate that the fits are reasonable and are also shown in Fig. 1 (a).

Uncertainty in the ξ_{peak} values due to the choice of fitting range was added in quadrature to the total systematic uncertainty. It was evaluated by changing the fit range to $\mu_\xi \pm 0.9$ and $\mu_\xi \pm 1.1$, leading maximally to a $^{+0.14}_{-1.31}\%$ systematic effect. The largest and only other source

[a]The word "electron" is used as a generic term for electrons and positrons.

contributing more than 1% to the systematic uncertainty was the CAL energy scale, leading to a $^{+0.58}_{-2.86}\%$ effect. The extracted values of $\xi_{\rm peak}$ are given in Table 1 and are observed to increase as the energy scale or θ_c increases.

Assuming $\Lambda_{\rm eff}$ is constant within the range of energies probed, Eq. 1 can be directly fit to the $\xi_{\rm peak}$ data, treating $\Lambda_{\rm eff}$ as a free parameter. In the case where only the ZEUS γp data with $\theta_c = 0.23$ were considered, shown in Fig. 1 (b), the best fit value was found to be $\Lambda_{\rm eff} = 275 \pm 4({\rm stat.})^{+4}_{-8}({\rm syst.})$ MeV. The χ^2/dof of the fit was 0.70, indicating a good fit. When the global data set was considered, the best fit value was found to be $\Lambda_{\rm eff} = 246 \pm 3({\rm stat.} \oplus {\rm syst.})$ MeV. In the global fit, all uncertainties were treated as uncorrelated. The χ^2/dof of the fit, with this simplistic error treatment, was 2.2, indicating some discrepancy. The globally extracted value of $\Lambda_{\rm eff}$ is not consistent with that extracted from the ZEUS data alone.

The energy dependence of $\Lambda_{\rm eff}$ was studied by using Eq. 1 to map each $\xi_{\rm peak}$ value to a corresponding value of $\Lambda_{\rm eff}$. The results, given in Table 1 and shown in Fig. 1 (c) as a function of $E_{\rm jet}$, show no evidence that $\Lambda_{\rm eff}$ is dependent on the energy scale. Also shown are CDF data [7], ZEUS *ep* data [6], OPAL data [8], and L3 data [9]. A weak dependence was observed in the CDF data [7], which span a wider range of energy scales. However, the data do suggest that the value of $\Lambda_{\rm eff}$ is weakly dependent on θ_c. Specifically, Table 1 shows that the values of $\Lambda_{\rm eff}$ extracted from the wider cone data tend to be systematically larger. This behaviour was also observed by the CDF collaboration [7]. Both the θ_c and $E_{\rm jet}$ dependence seen by CDF would contribute to the discrepancy observed when fitting Eq. 1 to the global data set.

The ξ distributions were also fitted using the predicted limiting spectrum, according to Eq. 3. The quantities K and $\Lambda_{\rm eff}$ were treated as free parameters during the fit. The χ^2/dof values of the fits lie between 0.34 and 2.72. Typically, in each $E_{\rm jet}$ bin, the χ^2/dof increases as θ_c does. The χ^2/dof values indicate that, while the theory does describe many of the features of the data in the fitting ranges, there are differences. Specifically, the rising edges of the ξ peaks are well described. However, the upper tails of the distributions are not adequately reproduced. This is likely due to the specific MLLA regularisation scheme used which causes the partons to be cut-off at $p_T^{\rm rel,pl} = \Lambda_{\rm eff}$, whereas the hadrons in the data are not. This leads to an intrinsic discrepancy between data and theory.

The values of $\Lambda_{\rm eff}$ extracted from the MLLA fits are given in Table 1. The results are in reasonable agreement with those extracted from the $\xi_{\rm peak}$ data, although the values extracted using the MLLA fit have larger uncertainties. The value of $\Lambda_{\rm eff}$ from the MLLA method with $\theta_c = 0.23$ and averaged over $E_{\rm jet}$, weighting each data point based only on its statistical precision, is $\Lambda_{\rm eff} = 304 \pm 6({\rm stat.})^{+8}_{-32}({\rm syst.})$ MeV.

Values of $\kappa_{\rm ch}$ were extracted from the fitted K values using Eq. 3 and the values of $\epsilon_{\rm g}$ predicted for each $E_{\rm jet}$ bin by the Pythia model. The $\epsilon_{\rm g}$ values were roughly constant in $E_{\rm jet}$, at $\epsilon_{\rm g} \approx 0.2$. The $\kappa_{\rm ch}$ values are given in Table 1. The total uncertainty is dominated by the theoretical uncertainty associated with the next-to-MLLA correction factors. The $\kappa_{\rm ch}$ data suggest a weak dependence on θ_c. Specifically, as θ_c increases, so too does the central value of $\kappa_{\rm ch}$. This is significant when the high degree of statistical correlation between the three θ_c samples and the bin-to-bin correlation in the systematic and theoretical uncertainties are taken into consideration. The value of $\kappa_{\rm ch}$, measured with $\theta_c = 0.23$ and averaged over $E_{\rm jet}$, weighting the data points based on their statistical precision, was $\kappa_{\rm ch} = 0.55 \pm 0.01({\rm stat.})^{+0.03}_{-0.02}({\rm syst.})^{+0.11}_{-0.09}({\rm theo.})$.

A more detailed account of this analysis can be found at the pre-print [10] and slides [11].

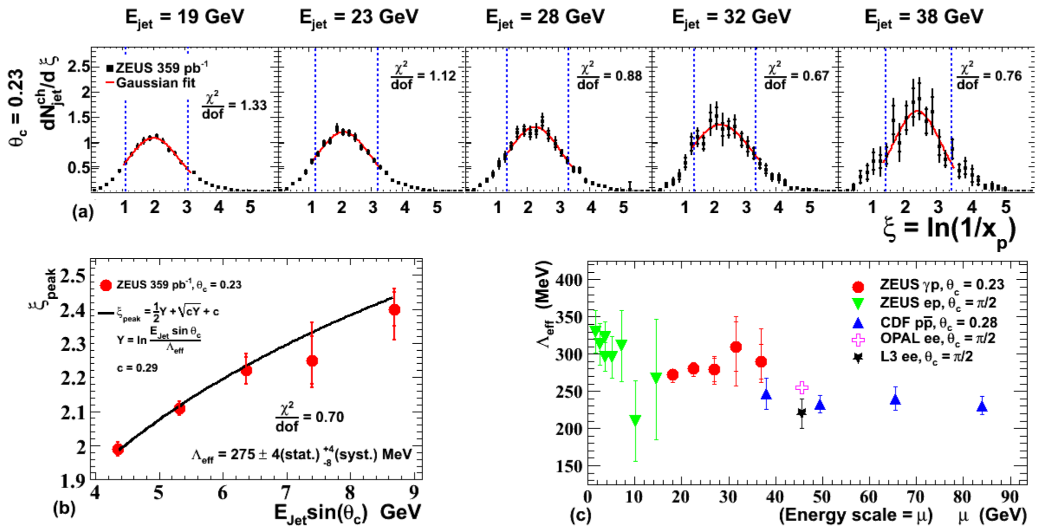

Figure 1: (a) The ξ distributions in the five $E_{\rm jet}$ bins with $\theta_c = 0.23$. The ZEUS data are shown by the solid squares. Gaussian functions (solid line) have been fitted to the data within the regions indicated (dashed lines). The χ^2/dof of each fit is given on the plot. (b) $\xi_{\rm peak}$ as a function of $E_{\rm jet} \sin\theta_c$. The ZEUS γp data are shown by the solid circles and fitted to Eq. 1. (c) $\Lambda_{\rm eff}$ as a function of energy scale, μ. The ZEUS γp data are shown by the solid circles. Also shown are data from ZEUS(ep) [6], OPAL(ee) [8], L3(ee) [9] and CDF(pp) [7]. For all, the inner error bars on the ZEUS γp points represent the statistical uncertainty. The outer error bars represent the statistical plus systematic uncertainties added in quadrature for all data sets

$E_{\rm jet}$ (GeV)	θ_c	$\xi_{\rm peak}$	$\Lambda_{\rm eff}$ (MeV)	$\kappa_{\rm ch}$
19	0.23	$1.99 \pm 0.01 \; ^{+0.02}_{-0.02}$	$272 \pm 5 \; ^{+6}_{-8}$	$0.54 \pm 0.01 \; ^{+0.03}_{-0.02} \; ^{+0.11}_{-0.09}$
	0.28	$2.10 \pm 0.01 \; ^{+0.01}_{-0.01}$	$280 \pm 4 \; ^{+5}_{-5}$	$0.59 \pm 0.01 \; ^{+0.03}_{-0.01} \; ^{+0.12}_{-0.10}$
	0.34	$2.20 \pm 0.01 \; ^{+0.01}_{-0.01}$	$289 \pm 4 \; ^{+6}_{-5}$	$0.63 \pm 0.01 \; ^{+0.03}_{-0.02} \; ^{+0.12}_{-0.10}$
23	0.23	$2.11 \pm 0.02 \; ^{+0.02}_{-0.01}$	$280 \pm 7 \; ^{+6}_{-7}$	$0.56 \pm 0.01 \; ^{+0.03}_{-0.02} \; ^{+0.11}_{-0.09}$
	0.28	$2.21 \pm 0.02 \; ^{+0.02}_{-0.01}$	$291 \pm 9 \; ^{+3}_{-11}$	$0.60 \pm 0.01 \; ^{+0.04}_{-0.02} \; ^{+0.12}_{-0.10}$
	0.34	$2.32 \pm 0.02 \; ^{+0.02}_{-0.01}$	$297 \pm 8 \; ^{+3}_{-9}$	$0.63 \pm 0.01 \; ^{+0.04}_{-0.02} \; ^{+0.13}_{-0.10}$
28	0.23	$2.22 \pm 0.04 \; ^{+0.03}_{-0.02}$	$279 \pm 16 \; ^{+8}_{-11}$	$0.55 \pm 0.01 \; ^{+0.04}_{-0.01} \; ^{+0.11}_{-0.09}$
	0.28	$2.34 \pm 0.03 \; ^{+0.02}_{-0.02}$	$282 \pm 14 \; ^{+8}_{-9}$	$0.59 \pm 0.01 \; ^{+0.04}_{-0.04} \; ^{+0.11}_{-0.09}$
	0.34	$2.44 \pm 0.04 \; ^{+0.04}_{-0.01}$	$292 \pm 17 \; ^{+5}_{-17}$	$0.61 \pm 0.01 \; ^{+0.04}_{-0.02} \; ^{+0.12}_{-0.10}$
32	0.283	$2.25 \pm 0.07 \; ^{+0.09}_{-0.05}$	$310 \pm 33 \; ^{+22}_{-41}$	$0.56 \pm 0.02 \; ^{+0.04}_{-0.04} \; ^{+0.11}_{-0.09}$
	0.28	$2.36 \pm 0.06 \; ^{+0.10}_{-0.03}$	$321 \pm 29 \; ^{+14}_{-49}$	$0.59 \pm 0.02 \; ^{+0.04}_{-0.04} \; ^{+0.11}_{-0.09}$
	0.34	$2.56 \pm 0.06 \; ^{+0.07}_{-0.05}$	$283 \pm 24 \; ^{+21}_{-28}$	$0.61 \pm 0.02 \; ^{+0.04}_{-0.03} \; ^{+0.12}_{-0.10}$
38	0.23	$2.40 \pm 0.05 \; ^{+0.04}_{-0.08}$	$290 \pm 23 \; ^{+38}_{-16}$	$0.56 \pm 0.03 \; ^{+0.05}_{-0.06} \; ^{+0.11}_{-0.09}$
	0.28	$2.50 \pm 0.08 \; ^{+0.07}_{-0.18}$	$301 \pm 37 \; ^{+48}_{-33}$	$0.58 \pm 0.03 \; ^{+0.04}_{-0.04} \; ^{+0.11}_{-0.09}$
	0.34	$2.59 \pm 0.07 \; ^{+0.08}_{-0.15}$	$319 \pm 36 \; ^{+31}_{-38}$	$0.61 \pm 0.03 \; ^{+0.03}_{-0.05} \; ^{+0.12}_{-0.10}$

Table 1: $\xi_{\rm peak}$, $\Lambda_{\rm eff}$ and $\kappa_{\rm ch}$ values in the five $E_{\rm jet}$ bins using the three θ_c values. The statistical, systematic and theoretical uncertainties are also given.

4 Bibliography

References

[1] Y.L. Dokshitzer, V.S. Fadin and V.A. Khoze, Phys. Lett. **B115** 242 (1982);
A.H. Mueller, Nucl. Phys. **B228** 351 (1983);
A.H. Mueller, Nucl. Phys. **B241** 141 (1984);
E.D. Malaza and B.R. Webber, Phys. Lett. **B149** 501 (1984);
Y.L. Dokshitzer, V.A. Khoze and S.I. Troian, Z. Phys. **C55** 107 (1992).

[2] Y.I. Azimov et al, Z. Phys. **C27** 65 (1985).

[3] V.A. Khoze, W. Ochs and J. Wosiek, arXiv:hep-ph/0009298.

[4] S. Lupia and W. Ochs, Phys. Lett. **B418** 214 (1998);
I.M. Dremin and J.W. Gary, Phys. Lett. **B459** 341 (1999);
S. Catani et al, Nucl. Phys. **B383** 419 (1992).

[5] ZEUS Coll., M. Derrick et al, Phys. Lett. **B297** 404 (1992);
ZEUS Coll., U. Holm(ed.), *The ZEUS Detector*. Status Report (unpublished), DESY (1993), available on `http://www-zeus.desy.de/bluebook/bluebook.html`.

[6] ZEUS Coll., M. Derrick et al., Z. Phys. **C67** 94 (1995);
ZEUS Coll., J. Breitweg et al., Eur. Phys. J. **C11** 251 (1999).

[7] CDF Coll., D. Acosta et al., Phys. Rev. **D68** 012003 (2003).

[8] OPAL Coll., M.Z. Akrawy et al., Phys. Lett. **B247** 617 (1990).

[9] L3 Coll., B. Adeva et al., Phys. Lett. **B259** 199 (1991).

[10] ZEUS Coll., S. Chekanov et al., arXiv:hep-ex/0904.3466.

[11] Slides :
`http://indico.cern.ch/materialDisplay.py?contribId=290&sessionId=3&materialId=slides&confId=53294`